Parametrically excited sectorial oscillation of liquid drops floating in ultrasound

C. L. Shen, W. J. Xie, and B. Wei*

Department of Applied Physics, Northwestern Polytechnical University, Xi'an 710072, People's Republic of China

(Received 21 September 2009; revised manuscript received 4 February 2010; published 9 April 2010)

We report experiments in which the nonaxisymmetric sectorial oscillations of water drops have been excited using acoustic levitation and an active modulation method. The observed stable sectorial oscillations are up to the seventh mode. These oscillations are excited by parametric resonance. The oblate initial shape of the water drops is essential to this kind of excitations. The oscillation frequency increases with mode number but decreases with equatorial radius for each mode number. The data can be well described by a modified Rayleigh equation, without the use of additional parameters.

DOI: 10.1103/PhysRevE.81.046305 PACS number(s): 47.55.D−, 43.25.+y, 68.03.Cd

I. INTRODUCTION

Since the 19th century, the dynamics of liquid drops has aroused great interest in various fields, such as hydrodynamics, aerography, and materials physics, with focus on underlying mechanism [1–6], practical applications [7–9] as well as models in astral and nuclear physics [10–12]. The small amplitude oscillation of free drops in vacuum was first treated by Rayleigh [2] using spherical harmonic bases, and the oscillation frequency of the normal modes was derived in linear approximation. Lamb [13] extended this analysis to the case of a droplet oscillating in an immiscible fluid. With the development of various containerless processing methods, these predictions were experimentally verified and applied to the noncontact measurement of the surface tension of liquids, especially to the undercooled or reactive melts [7,9].

Acoustic levitation suspends objects by an acoustic radiation pressure arising from the nonlinear effect of intensive ultrasound [14]. It can be applied to the conductors as well as nonconductors, such as ceramics, organic materials, and molecular fluid [15] because it has no special requirements for the electromagnetic property of the samples. The axisymmetric oscillation of acoustically levitated liquid drop in an immiscible fluid has been extensively investigated. Measured oscillation frequencies are in reasonable agreement with theoretical results from linear approximation [16]. An oblate distortion of the levitated drop tends to increase the oscillation frequency of the axisymmetric mode [17]. The internal circulation of the fluid within the drop was visualized by tracing particles illuminated by a sheet light [16,17]. The interaction of different oscillation modes was revealed by an image analysis method [18]. The effect of surfactant on the large amplitude axisymmetric oscillation was investigated in microgravity [19]. The axisymmetric oscillations have been numerically calculated with various methods, such as the marker-and-cell method [20], the boundary element method [21], and the Galerkin/finite-element method [22]. These calculations mainly focus on the oscillation frequency and shape evolution of the drops. There is a reasonable agreement between the theoretical analysis and experimental observations.

As compared with the extensive investigations *on* axisymmetric oscillations, there are only few studies on the nonaxisymmetric oscillation of a free drop. Examples include the nonaxisymmetric oscillations of drops supported on substrates and excited by mechanic, electromagnetic, or thermal disturbances [23–25]. These oscillations are complicated because of the confined interface, the hysteresis of the contact line of the liquids, or the rapid evaporation of liquids. In this work, we report the excitation of sectorial oscillation—a category of nonaxisymmetric oscillation—of water drops using acoustic levitation and an active modulation method. The dependence of the sectorial oscillation frequency on the drop parameters is investigated.

II. EXPERIMENTAL METHOD

The experimental setup is schematically shown in Fig. 1. The single-axis acoustic levitator is actuated by a piezoelectric (PZT) transducer, which works at a frequency of about 22 kHz. The ultrasound forms a standing wave between the emitter and the curved reflector. The sample can be confined in a potential well around the pressure node of this standing

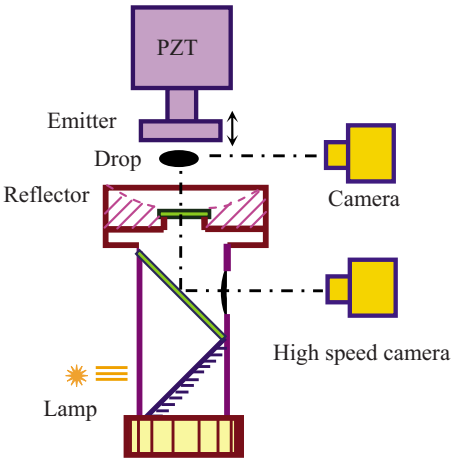

FIG. 1. (Color online) Experimental setup. The levitated water drop was excited into oscillations by modulation of the voltage applied to the transducer. The bottom view images were recorded by a high speed camera. After the modulation was turned off, the side view image was recorded by another camera.

*Corresponding author; bbwei@nwpu.edu.cn

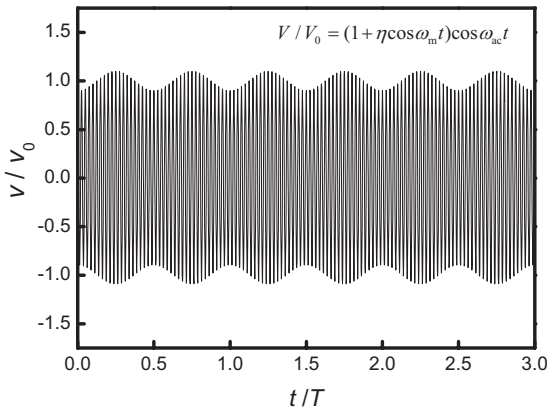

FIG. 2. Active modulation of the electric voltage applied to the transducer. In this plot, the modulation amplitude η is 0.1, the modulation frequency is 100 Hz ($\omega_m=200\pi$), and the ultrasound frequency is 20 kHz ($\omega_{ac}=40000\pi$).

wave. The gravity of the sample is counteracted by the sum of the acoustic radiation force on the whole surface of the levitated sample. The curved reflector introduces a sufficient lateral confinement to prevent the escape of the sample. More details on the single-axis acoustic levitator can be found elsewhere [26].

In the experiments, a water drop about 5 mm in diameter was levitated at the second resonant state of the acoustic field. To excite the levitated water drop into oscillation, the electric voltage V applied to the PZT transducer is actively modulated in the form of $V=V_0(1+\eta\cos\omega_m t)\cos\omega_{ac}t$, as shown in Fig. 2, where ω_m and ω_{ac} are the angular frequencies of the modulation signal and the ultrasound, respectively, η the ratio of the modulation amplitude to the initial electric voltage V_0. At high sound pressure level (SPL), the liquid drop deforms into an axisymmetric oblate shape [27]. Under this condition, a small variation in SPL will not significantly change the levitation status. Therefore, high SPL (>163 dB) and small amplitude modulation ($\eta\sim0.1$) were adopted in the experiments.

By tuning the modulation frequency upward with an increment of 0.5 Hz, different oscillation modes can be excited within narrow bands less than 10 Hz wide. Through a window at the center of the reflector, the bottom view images (384×384) of the oscillating drop were recorded by a Redlake HG 100 K high speed camera at a rate of 2000–5000 frames/s, and the oscillation frequency can be obtained from the recorded sequence of images. After the cessation of the modulation, the drop becomes stationary in a few seconds. The side view image of this stationary drop was recorded by another camera, which was taken as the equilibrium shape. The equatorial radius can be obtained from the side view image (1280×1024) with accuracy better than 1%. The mass of the drop was obtained by measuring the weight increase in a sponge after absorbing the water drop. Each drop is used for only one measurement of the oscillation frequency.

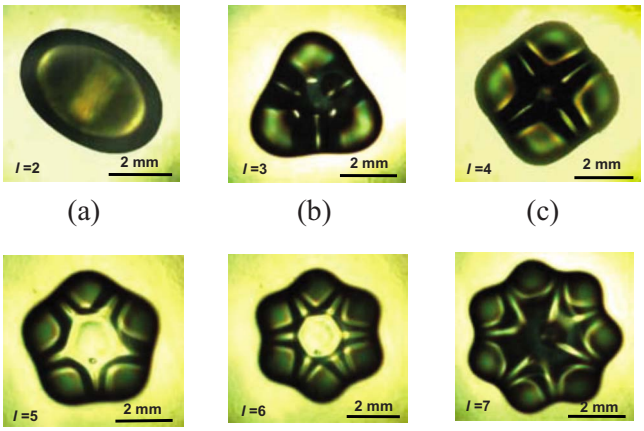

FIG. 3. (Color online) Typical two- to seven-lobed patterns of acoustically levitated water drop. These are bottom view images of the oscillating drops, shown at maximum deviation amplitude.

III. RESULTS AND DISCUSSIONS

A. Sectorial oscillation patterns

The typical patterns observed in the experiments are illustrated in Fig. 3, which are the bottom view images of the oscillating drops, shown at maximum deviation amplitude. These patterns are characterized by l ($l=2-7$) equally spaced lobes. During the oscillation, these lobes stretch out and contract back alternately. As an example, a typical seven-lobed oscillation is shown in Fig. 4, where the five selected images correspond to the phases of 0, $\pi/2$, π, $3\pi/2$, and 2π in one period of evolution, respectively. The oscillation frequencies of the drops shown in Figs. 3(a)–3(f) are measured to be 30.5, 53, 90, 107, 141, and 154 Hz respectively, which are exactly half of the corresponding modulation frequencies. More detailed information concerning the two- to seven-lobed mode of oscillation can be found in supplementary movies [28].

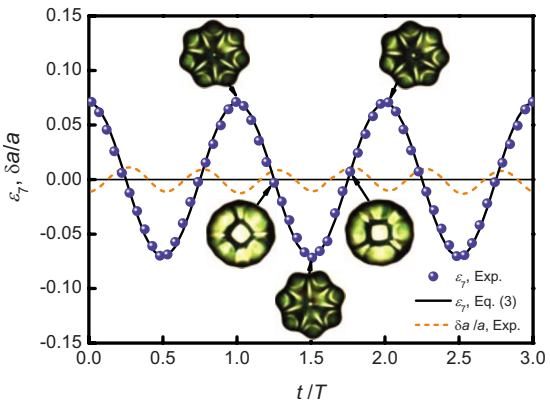

FIG. 4. (Color online) Evolution of a seventh mode sectorial oscillation. The dots are experimental results of ε_7 acquired from the recorded images. The solid line is the prediction of ε_7 by Eq. (3) with $\varepsilon_{07}=0.07$ and $\omega_7=308\pi$. The dashed lines shows the variation of a in the oscillation as the result of modulated acoustic field. The period of this sectorial oscillation T is 6.5 ms.

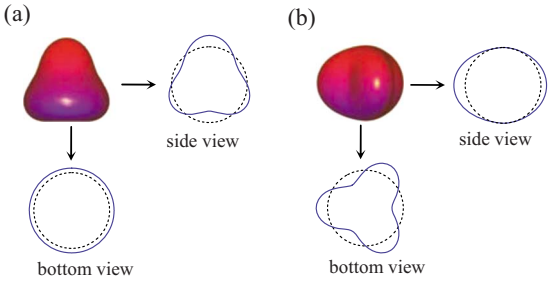

FIG. 5. (Color online) Axisymmetric oscillation and sectorial oscillation of a spherical drop. (a) Side view and bottom view of the third mode axisymmetric oscillation. (b) Side view and bottom view of the third mode sectorial oscillation. The oscillation amplitudes are 0.3. The dashed lines represent the equilibrium spherical shape of the drop.

The oscillation of a free drop can be decomposed on the spherical harmonics basis [2]. According to the degree l and order m of the spherical harmonics $Y_{lm}(\theta,\varphi)$, the oscillation modes are classified into three categories [29]: zonal ($m=0$), tesseral ($l\neq m\neq 0$), and sectorial ($l=m\neq 0$). The first category is referred to as the axisymmetric oscillation and the others are nonaxisymmetric oscillation. Axisymmetric oscillation can be well represented by the side view images, while the sectorial oscillation is mainly characterized by the bottom view images. Examples of the two categories of oscillation are schematically shown in Fig. 5. From the characteristics of bottom view images in Fig. 3, these oscillations observed in our experiments can be identified to be the second to seventh mode sectorial oscillations.

Theoretically, the lth mode sectorial oscillation of a deformed drop is described as

$$r(\theta,\varphi,t) = r_0(\theta)[1 + c_l Y_{ll}(\theta,\varphi)\cos\ \omega_l t], \tag{1}$$

where $r_0(\theta)$ represents the equilibrium shape of the initially flattened drop, and the second term in the rectangular brackets is the oscillating part with angular frequency ω_l and oscillation amplitude c_l. By inserting $\theta=\pi/2$ into Eq. (1), the outline of the bottom view image, i.e., the equatorial flange of the drop, can be expressed as

$$r(\varphi,t) = a[1 + \varepsilon_l(t)\cos(l\varphi + \varphi_0)], \tag{2}$$

where

$$\varepsilon_l(t) = \varepsilon_{0l}\cos(\omega_l t). \tag{3}$$

In Eqs. (2) and (3), a is the equatorial radius of drop at equilibrium state, $\varepsilon_l(t)$ the transient deviation amplitude of liquid drop, and ε_{0l} the oscillation amplitude of $\varepsilon_l(t)$.

To compare the experimental observations with the sectorial oscillation predicted by Eq. (1), the outlines of the bottom view images were extracted. The extracted outlines of the images in Fig. 3 are presented in Fig. 6 as the blue dots. These dots are fitted with $r(\varphi)=a[1+\varepsilon_{0l}\cos(l\varphi+\varphi_0)]$ and the results are plotted as the red solid lines. The good agreement between the dots and the solid lines confirms that these

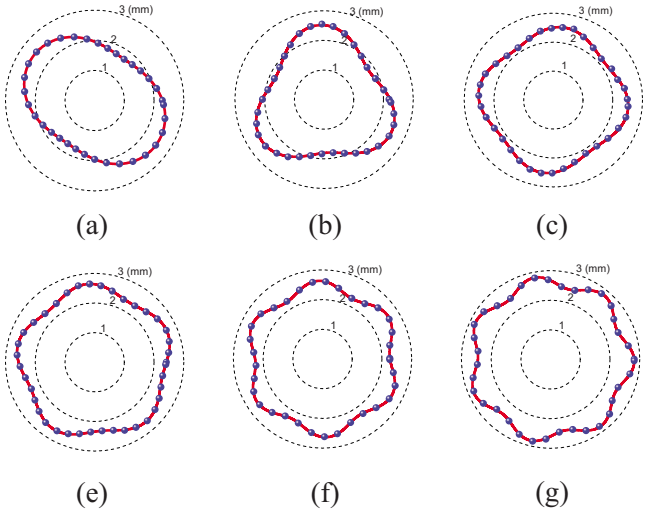

FIG. 6. (Color online) Outlines of the water drop images displayed in Fig. 3. The blue dots are the experimentally extracted edge points by an image processing method. The red solid lines are the fitted outlines with $r(\varphi)=a[1+\varepsilon_{0l}\cos(l\varphi+\varphi_0)]$.

oscillations are sectorial oscillation. The oscillation amplitudes ε_{0l} are determined as 0.20, 0.17, 0.08, 0.07, 0.08, and 0.07 for the second to seventh mode sectorial oscillations, respectively.

The time evolution of ε_l and φ_0 can be obtained by fitting the outlines of a sequence of continuously recorded images. The result of ε_7 for the seventh mode sectorial oscillation is plotted as dots in Fig. 4. These dots are found to agree well with the prediction of Eq. (3) with $\varepsilon_{07}=0.07$ and $\omega_7=308\pi$, which is shown as the solid line. According to the fitted result of φ_0, the rotation rate of the drop is determined to be less than one round per second, and its effect on the sectorial oscillation is negligible.

B. Sectorial oscillation frequency

For the free oscillation of a spherical drop with infinitesimal amplitude, the natural frequency of the mode (l,m) is given by Rayleigh equation [2],

$$f_R = \frac{1}{2\pi}\sqrt{\frac{\sigma}{\rho R^3} l(l-1)(l+2)}, \tag{4}$$

where σ, ρ, and R are the surface tension, density, and radius of the drop, respectively. For an initially deformed drop, such as the case in the present experiments, the natural frequency deviates from the value predicted with Eq. (4). Moreover, their values for the modes with the same degree l but different order m are different from each other, according to the results in previous investigations [30,31].

In our experiments, when the active modulation is turned off, the liquid drop enters the free decaying stage. The decay time decreases with the increase of l. It takes about 1.5 s for a typical second mode oscillation to decay to 5% of its initial amplitude, and about 0.3 s for a seventh mode. The oscillation frequency does not change from before until after the cessation of modulation, indicating that the drop oscillates at

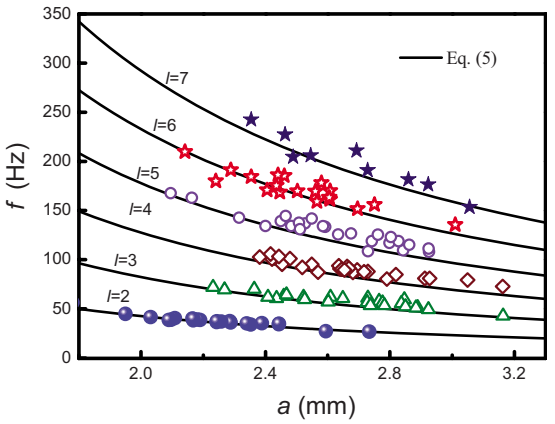

FIG. 7. (Color online) Sectorial oscillation frequencies of the acoustically levitated water drops. The various symbols are the measured data for $l=2-7$, respectively. a is the initial equatorial radius of the drop. The solid lines are the calculated results with Eq. (5).

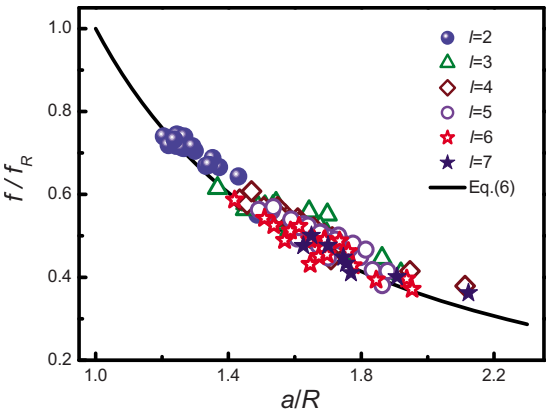

FIG. 8. (Color online) Oscillation frequency normalized with corresponding value calculated by Rayleigh's equation. R is the radius of water drop when it takes a spherical shape.

its natural frequency. The modulation only helps to surmount the dissipation of energy.

To explore the relationship between the natural frequency and the parameters of deformed drops, the sectorial oscillation frequencies were measured for different modes as well as different initial equatorial radii a, see Fig. 7. The frequency increases with increasing l, whereas it decreases with increasing a.

The dependence of the measured oscillation frequency on drop size and oscillation mode is found to be well described with a modified expression of Rayleigh equation by substituting R with a,

$$f = \frac{1}{2\pi}\sqrt{\frac{\sigma}{\rho a^3} l(l-1)(l+2)}. \tag{5}$$

Equation (5) is depicted in Fig. 7 as solid curves for $l=2-7$. In this calculation, the density and surface tension of water drops at the room temperature of 302 K are adopted, and the values are 0.071 N/m and 0.996×10^3 kg/m^3, respectively. According to Eq. (5), the sectorial oscillation frequencies depend mainly on the equatorial radius of the drop. It is probably because the sectorial oscillation is mainly horizontal. According to Eq. (1), the oscillating term $c_l r_0(\theta) Y_{ll}(\theta,\varphi)\cos\omega_l t$ is proportional to $r_0(\theta)\sin^l\theta$, which has maximum value at the equatorial plane and is zero at the polar point.

The sectorial oscillation frequency of a deformed drop can be normalized with respect to the corresponding Rayleigh frequency as

$$f/f_R = (a/R)^{-3/2}, \tag{6}$$

where the ratio a/R indicates the deformation extent of the drop. The normalized result for the measured oscillation frequencies agrees well with Eq. (6), as shown in Fig. 8. It is clear that the sectorial oscillation frequency decreases with increasing deformation. As a/R approaches 2.0, the frequency of the sectorial oscillation declines to about 35% ofthe corresponding Rayleigh frequency. This result is different from that of axisymmetric oscillation, according to the investigation of Trinh *et al.* [17]. In their experiment, the frequency of axisymmetric oscillations increases with the increasing ratio a/R.

C. Excitation of sectorial oscillations

To understand how the sectorial oscillation comes into being, we analyze the static and dynamic conditions of the levitated drop. For a stationary drop, the pressures on the surface are balanced as $P_{\rm in}+P_{\rm g}=P_{\rm rad}+P_\sigma+P_0$, where $P_{\rm in}$ is the inner static pressure, $P_{\rm g}=\rho g(z_0-z)$ the gravity-induced pressure, $P_{\rm rad}$ the acoustic radiation pressure, $P_\sigma=\sigma(1/R_1+1/R_2)$ the curvature-induced capillary pressure, and P_0 the ambient pressure. When the electric voltage applied to the PZT transducer is actively modulated as $V=V_0(1+\eta\cos\omega_{\rm m}t)\cos\omega_{\rm ac}t$, the incident acoustic pressure $p_{\rm i}$ varies in a similar form with excess pressure $\Delta P_{\rm rad}$ ($\propto\eta\cos\omega_{\rm m}t$).

It is interesting that a nonaxisymmetric oscillation occurs in an axisymmetric force field, and the frequency is half of the modulation frequency. Actually, it is excited by parametric excitation [32,33]. The oscillation is not directly driven by external force. Instead, parameters influencing the natural frequency act as the bridge.

According to Eq. (5), the sectorial oscillation of the acoustically levitated drop can be expressed in a general form,

$$\ddot{\varepsilon}_l + \omega_l^2 \varepsilon_l = 0, \tag{7}$$

where

$$\omega_l^2 = \frac{\sigma l(l-1)(l+2)}{\rho a^3}. \tag{8}$$

As the acoustical radiation pressure is modulated at a frequency of $\omega_{\rm m}$, the equatorial radius is perturbed with the same frequency as

$$a = a_0(1 + \Delta \cos \omega_m t), \tag{9}$$

where a_0 is the mean value of a. This has been verified in the experiments. As for the seventh sectorial oscillation, the variation, $\delta a/a = \Delta \cos \omega_m t$, is plotted as the dashed line in Fig. 4. By inserting Eq. (9) into Eq. (8) and omitting the high order terms of Δ, the oscillation equation becomes

$$\ddot{\varepsilon}_l + \omega_{0l}^2(1 + 3\Delta \cos \omega_m t)\varepsilon_l = 0, \tag{10}$$

where ω_{0l} is the natural frequency of drop for $a = a_0$. This is the classical parametric oscillation equation [32]. One solution of the Eq. (10) is

$$\varepsilon_l = \varepsilon_0 e^{st} \cos(\omega_l + \xi/2), \tag{11}$$

Where $s = \sqrt{9\omega_l^2\Delta^2/16 - \xi^2/4}$. When the active modulation frequency is $\omega_m = 2\omega_l + \xi$ with $|\xi| < 3\omega_l\Delta/2$, s is positive and ε_l will increase with time. Therefore the sectorial oscillation is excited. As for the seventh mode sectorial oscillation illustrated in Fig. 4, the values of Δ and ω_7 are 0.01 and 308π, respectively. To excite this sectorial oscillation, $|\xi|$ should be less than 3.2π, and the corresponding modulation frequency should be 308 ± 1.6 Hz. This agrees reasonably with the experimental result of about 308 ± 1 Hz.

The deformation of liquid drop is essential for the excitation of the large amplitude sectorial oscillation. It makes the natural frequency of the sectorial oscillation different from that of the corresponding axisymmetric oscillation, which allows sectorial oscillation—rather than the axisymmetric oscillation—to be excited to large amplitude by resonance.

In the experiments, sectorial oscillations up to the seventh mode were successfully excited. We believe two aspects of our experimental setup are important for rendering these excitations possible. First, the levitation force and stability of the levitator are guaranteed with optimized geometric parameters [34]. Second, during the oscillation, the energy dissipation is weak for the low viscosity liquids immersed in air. The viscosity of water is about 0.9 mPa s at room temperature. The dragging effect of surrounding air is slight, as the density of air is negligible as compared with that of water.

IV. CONCLUSIONS

The sectorial oscillations of liquid drops are parametrically excited by actively modulating the acoustic field. The sectorial oscillation frequency decreases with increasing equilibrium radius and can be described by a modified Rayleigh equation [Eq. (5)]. The oblate initial shape makes the natural frequency of sectorial oscillation modes different from that of corresponding axisymmetric modes, and enables parametric excitation of these oscillations. The relatively low energy dissipation accounts for the observation of high *mode oscillations* in the experiment. This study enriches our knowledge on drop oscillation. One prospective application is to measure the surface tension of liquids in a noncontact manner using the modified Rayleigh equation. We believe more applications can be found in the study of liquid properties and the influence of fluid convection on the containerless processing of materials.

ACKNOWLEDGMENTS

The work was supported by the National Natural Science Foundation of China (Grants No. 50121101, No. 50395105, and No. 50301012), and the Foundation for the Author of National Excellent Doctorial Dissertation of China. The authors are grateful to Dr. Y. J. Lü, Dr. H. P. Wang, Mr. Z. Y. Hong and Mr. B. C. Luo for beneficial discussions.

[1] J. A. F. Plateau, *Annu. Rep. Board Regents Smithson. Inst.* 207–285 (1863).
[2] L. Rayleigh, Proc. R. Soc. London **29**, 71 (1879).
[3] T. Gilet and J. W. M. Bush, Phys. Rev. Lett. **102**, 014501 (2009).
[4] E. Villermaux and B. Bossa, Nat. Phys. **5**, 697 (2009).
[5] S. Courty, G. Lagubeau, and T. Tixier, Phys. Rev. E **73**, 045301(R) (2006).
[6] J. B. Bostwick and P. H. Steen, Phys. Fluids **21**, 032108 (2009).
[7] T. Ishikawa, P. F. Paradis, N. Koike, and Y. Watanabe, Rev. Sci. Instrum. **80**, 013906 (2009).
[8] R. T. Collins, J. J. Jones, M. T. Harris, and O. A. Basaran, Nat. Phys. **4**, 149 (2008).
[9] I. Egry, G. Lohoefer, and G. Jacobs, Phys. Rev. Lett. **75**, 4043 (1995).
[10] M. Shibata and Y. Sekiguchi, Phys. Rev. D **71**, 024014 (2005).
[11] V. G. Kartavenko, K. A. Gridnev, and W. Greiner, Phys. Atom. Nucl. **65**, 637 (2002).
[12] R. J. A. Hill and L. Eaves, Phys. Rev. Lett. **101**, 234501 (2008).
[13] H. Lamb, *Hydrodynamics*, 6th ed. (Cambridge University Press, Cambridge, England, 1932).
[14] L. V. King, Proc. R. Soc. London, Ser. A **147**, 212 (1934).
[15] E. H. Trinh, Rev. Sci. Instrum. **56**, 2059 (1985).
[16] E. H. Trinh, A. Zwern, and T. G. Wang, J. Fluid Mech. **115**, 453 (1982).
[17] E. H. Trinh and T. G. Wang, J. Fluid Mech. **122**, 315 (1982).
[18] E. H. Trinh, D. B. Thiessen, and R. G. Holt, J. Fluid Mech. **364**, 253 (1998).
[19] R. E. Apfel *et al.*, Phys. Rev. Lett. **78**, 1912 (1997).
[20] G. B. Foote, J. Comput. Phys. **11**, 507 (1973).
[21] T. S. Lundgren and N. N. Mansour, J. Fluid Mech. **194**, 479 (1988).
[22] O. A. Basaran, J. Fluid Mech. **241**, 169 (1992).
[23] V. Kocourek, Ch. Karcher, M. Conrath, and D. Schulze, Phys. Rev. E **74**, 026303 (2006).
[24] H. Azuma and S. Yoshihara, J. Fluid Mech. **393**, 309 (1999).
[25] N. Yoshiyasu, K. Adachi, and R. Takaki, J. Phys. Soc. Jpn. **62**, 2314 (1993).
[26] W. J. Xie and B. Wei, Appl. Phys. Lett. **79**, 881 (2001).
[27] W. J. Xie and B. Wei, Phys. Rev. E **70**, 046611 (2004).

[28] See supplementary material at http://link.aps.org/supplemental/10.1103/PhysRevE.81.046305 for supplementary movies.
[29] R. Natarajan and R. A. Brown, J. Fluid Mech. **183**, 95 (1987).
[30] P. V. R. Suryanarayana and Y. Bayazitoglu, Phys. Fluids A **3**, 967 (1991).
[31] D. L. Cummings and D. A. Blackburn, J. Fluid Mech. **224**, 395 (1991).
[32] L. Landau and M. Lifshitz, *Mechanics*, 3rd ed. (Butterworth-Heinemann, Oxford, 1976).
[33] X. Noblin, A. Buguin, and F. Brochard-Wyart, Phys. Rev. Lett. **94**, 166102 (2005).
[34] W. J. Xie, C. D. Cao, Y. J. Lü, and B. Wei, Phys. Rev. Lett. **89**, 104304 (2002).